Seasonal cycles of a 3D marine ecosystem model in the North Indian Ocean: Sensitivity to biological process parameters

P.S.Swathi, M.K.Sharada, and K.S.Yajnik,

CSIR Centre for Mathematical Modeling and Computer Simulation (C-MMACS),
Wind Tunnel Road, Bangalore – 560 037, India
[Email-:swathi@cmmacs.ernet.in]

Parameter sensitivity studies are done at C-MMACS using a 3D coupled physical-biological-chemical model of the oceanic carbon cycle. This model is evaluated by using U.S. Joint Global Ocean Flux Studies (U.S. JGOFS) data, satellite data and buoy data for different values of a few of the parameters which influence the regeneration of ammonium and growth of zooplankton and hence the carbon flux across the air-sea interface. Important processes which affect the primary productivity and chlorophyll have been identified. A set of ecosystem parameters which have great potential for studying the marine productivity and carbon dioxide transfer in the Indian Ocean have been isolated in this study.

Introduction

North Indian Ocean has several interesting features. C^{14}-based seasonal primary productivity observed during JGOFS has the largest values in the Arabian Sea region (86 ± 5 to 137 ± 13 mmol C m^{-2} d^{-1}), values in other regions (Equatorial Pacific at 140°W, North Atlantic at 47°N, Central North Pacific at 24°N, Ross Sea and Antarctic Polar front zone) being significantly less (20 ± 2 to 107 ± 23 mmol C m^{-2} d^{-1}; Barber *et al*[1]). Arabian Sea also provides considerable seasonal and spatial diversity in physical forcing; SST observed during JGOFS cruises varied from 22 to 28°C, wind stress from 0.01 to 0.25 N m^{-2}, upwelling from -0.4 to 1.4 m d^{-1} and mixed layer depths ($\Delta\sigma_\theta = 0.013$) from 10 to 90 m. The diversity in the ecosystem response can be judged from the variation of surface nitrate from detectable level to ~15 µM and surface chlorophyll a from 0.1 to 0.8 mg m^{-3} (See Barber *et al*[1] for discussion on seasonal and spatial variability and for earlier references). Marra *et al*[2] have given a discussion of the time series of biological measurements at WHOI mooring site (15° 30', 61° 30'). There are also seasonal blooms associated with coastal upwelling of the West India Coastal Current and the East India Coastal Current. Large river water discharge and heavy precipitation, especially in the North Bay of Bengal, increase the static stability of the upper layers and suppress vertical fluxes that can bring up nutrients, except in mesoscale eddies and coastal upwelling regions and during episodic cyclonic disturbances. These differences in physical forcing govern the meridional and zonal variability of primary productivity (Prasanna Kumar *et al*[3,4]).

The spectrum of prognostic ecosystem models that have been developed so far is rather broad, ranging from the nitrogen–based model of Fasham *et al*[5] to the nitrogen-phosphorous-silicon-iron based model of Doney *et al*[6] and Moore *et al*[7,8]. Our approach to resolve the issue of appropriateness of the model has been different. With our ability to integrate biological and chemical models within OGCMs (Swathi *et al*[9], Sharada *et al*[10,11]), we are in a position to investigate the parameter sensitivity of integrated models and processes within them carefully.

Materials and Methods

Model

The physical model (Modular Ocean Model MOM2.2, Pacanowski[12]) and the biological model used in the numerical simulations are explained in detail in Swathi *et al*[9] and Sharada *et al*[11] and we provide only a summary here.

The computational domain for the physical model is 15°S to 27°N with resolution varying from 1° at 15°S to 0.4° north of equator, 37.6°E to 100°E with a resolution of 0.4° and there are 35 vertical levels (10m in the upper 120m). This horizontal resolution allows us to model reasonably the structures in Arabian Sea (AS) and Bay of Bengal

(BOB). The vertical resolution allows a good representation of upper ocean processes and light penetration which are essential for the ecosystem modeling.

The Pacanowski-Philander formulation (Pacanowski and Philander[13]) models mixed layer turbulence driven by strong monsoonal winds and winter cooling in the AS and also suppression by seasonal stratification in the BOB. The southern boundary is chosen at 15°S as our focus is on the North Indian Ocean. The sponge boundary condition is implemented by relaxing the model temperature and salinity in 5°S-15°S to climatology (Levitus *et al*[14]) on a time scale of 30 days. The model has a rigid lid at the upper surface and is forced by COADS monthly winds. Since sparse data create difficulties in prescribing surface heat flux, precipitation and river discharge with sufficient accuracy, we have adopted the indirect course of applying heat and salt flux at the surface generated from 50 year climatological runs and relaxing model surface temperature and salinity to monthly climatology (Levitus *et al*[14]) as explained in Swathi *et al*[9]. The model is spun for 50 years from rest with initial temperature and salinity profiles based on annual climatological values.

The biological model is based on the FDM[5] model for the euphotic zone and modified by Sarmiento *et al*[15] and Swathi *et al*[9] for break down and regeneration (conversion of organic nitrogen to inorganic nitrogen, especially ammonia by the action of bacteria) below the euphotic zone. The block diagram showing the components of the biological model and their interactions, and the governing equations are given in Appendix I. The model has seven components, namely, Phytoplankton (P), Zooplankton (Z), Bacteria (B), Ammonium (N_r), Nitrate (N_n), Detritus (D) and Dissolved Organic Nitrogen (N_d). The currency is nirtrogen. (i.e., Concentrations of state variables and fluxes between them are in units of nitrogen).

It is clear from the block diagram and the equations in the Appendix I, zooplankton is the controlling component. The abundance of zooplankton determines the uptake of phytoplankton, bacteria and detritus as well as the partitioning of the nitrogen between ammonium production in the euphotic zone and removal of organic matter $\gamma_4\mu_5 Z$ (Notation in Table 1) from the euphotic zone in the form of rapidly sinking detritus (detrital fraction of zooplankton mortality).

The parameters of the biological model used in Sharada *et al*[10], also called exp A in this study are given in Table 1. Table 2 provides the details of the parameter values used in the sensitivity analysis.

The Present study considerers the FDM[5] model with one modification. Exponential inhibition of nitrate uptake stipulated, following Wroblewski[16], in the nutrient kinetics model used in FDM[6] model is replaced by hyperbolic inhibition of nitrate uptake (Yajnik and Sharada[17]). Our nutrient kinetics model has three characteristics: (a) nitrate uptake, for a given nitrate concentration, decreases hyperbolically, possibly to a non-zero value, with increasing ammonium; (b) nitrate uptake in absence of ammonium and ammonium uptake are governed by Michaelis-Menten law and the latter is independent of nitrate concentration; and (c) the nutrient kinetic parameters are determined from observations of McCarthy *et al*[18]. This model has been shown to capture the ship-board observations of McCarthy *et al*[18] and also annual average primary productivity in the North Indian Ocean significantly better than the other nutrient kinetics models, including Wroblewski's model (Sharada *et al*[10]). The equations of the FDM[5] model with YS modifications are given in Appendix I.

With a view to delineate the effect of top down control by zooplankton and regeneration of ammonium through zooplankton, we have varied two sets of parameters. The first set governs the zooplankton grazing rate (maximum growth rate g and half-saturation constant of ingestion k_3). The second set governs the regeneration of ammonium by zooplankton (specific excretion rate μ_5, ammonium fraction of excretion γ_3 and detrital fraction of zooplankton mortality γ_4). The remaining five parameters related to zooplankton, twelve parameters related to phytoplankton, four related to bacteria and two related to detritus are kept at constant values given in Table 1. In all, nine cases are considered for various combinations as given in Table 2. Since each of these five parameters appears in a source/sink term in at least two ecosystem conservation equations, the net effect of changes of these parameters is not so obvious which illustrates the complexity of nonlinear models.

As indicated earlier, the parameters in exp A are identical to the ones in Sharada *et al*[11]. In exp B, the maximum growth rate of zooplankton (*g*) is reduced to 0.75/day while in exp C, ammonium

Table 1—Parameters of the biological model

Model Parameters	Values	Units
Related to Phytoplankton		
Initial Slope of P-I Curve, α	0.025	$d^{-1}/(Wm^{-2})$
Photosynthetically Active Radiation, PAR	0.4	
Light Attenuation by P, k_c	0.03	$m^{-1}/(mmolN/m^3)^{-1}$
Light Attenuation due to water, k_w	0.04	m^{-1}
Maximum Growth Rate Parameters, a	0.6	d^{-1}
b	1.066	
c	1.0	$°C^{-1}$
Exudation fraction, γ_1	0.05	
Specific Mortality Rate, μ_1	0.04	d^{-1}
Half-saturation for Nitrate Uptake, k_1	1.47	$mmolN/m^3$
Half-saturation for Ammonium Uptake, k_2	0.47	$mmolN/m^3$
Ammonium Inhibition Parameters, aa &bb	1.0, 3.0	$(mmolN)^{-1}$
Related to Zooplankton		
Maximum Growth Rate, g	1.0	d^{-1}
Assimilation Efficiency, γ_2	0.75	
Relative Preference of Z for P, p_1	0.4	
Relative Preference of Z for B, p_2	0.3	
Relative Preference of Z for N_p, p_3	0.3	
Half-saturation Rate for Ingestion, k_3	1.0	$mmolN/m^3$
Specific Excretion Rate, μ_2	0.1	d^{-1}
Specific Mortality Rate, μ_5	0.05	d^{-1}
Ammonium fraction of Z Excretion, γ_3	0.75	
Detrital fraction of Z Mortality, γ_4	0.33	
Related to Bacteria		
Maximum Growth Rate, V_b	2.0	d^{-1}
Specific Excretion Rate, μ_3	0.05	d^{-1}
Half-saturation Rate for Uptake, k_4	0.5	$mmolN/m^3$
Ammonium/DON Upatke Ratio, η	0.6	
Related to Detritus		
Breakdown Rate, μ_4	0.05	d^{-1}
Sinking Velocity, ω_s	-4.0	m/d

Table 2—Parameter values used in numerical expriments

Exp. No.	K3	G	μ_5	γ_3	γ_4
expA	1	1	0.05	0.75	0.33
expB	1	0.75	0.05	0.75	0.33
expC	1	1	0.05	0.5	0.33
expD	1	1	0.05	0.75	0.5
expE	1	1	0.1	0.75	0.33
expF	1.5	1	0.05	0.75	0.33
expG	0.6	0.6	0.05	0.75	0.33
expH	1	1	0.033	0.75	0.5
expI	1	1	0.1	0.75	0.5

fraction of zooplankton excretion (γ_3) is reduced to 0.5 (from 0.75 in exp A). In exp D, the detrital fraction of zooplankton mortality (γ_4) is increased to 0.5. In exp E, the rate of zooplankton mortality (μ_5) is increased to 0.1/day (0.05 in exp A) while in exp H, it is reduced to 0.033/day. In exp F, zooplankton growth is reduced by increasing half-saturation constant for grazing (k_3) to 1.5,

while in exp G, both k_3 and g are reduced. Exp I is similar to exp E with increased export of detrital matter out of the euphotic zone (0.5). All these changes in the parameter values lead to decrease in concentration of Zooplankton and Ammonium and also the regeneration of Ammonium by Zooplankton (as can be seen from Block diagram).

The coupled model run is started with dynamical fields from a 50 year run of the physical model. The 3D nitrate field is specified from climatology and other ecosystem fields are initialized to small non-zero values as explained in Swathi *et al*[9]. The ecosystem fields rapidly adjust to circulation and ecosystem dynamics in the upper ocean as shown in Sarmiento *et al*[15], Swathi *et al*[9], Sharada *et al*[11]. Therefore, the analysis of the fourth year for the upper ocean is considered adequate for our study. In addition, longer runs are actually

detrimental due to the closed nature of our simulations which do not have transport to/from other oceanic regions.

Results and Discussion

The coupled physical-biological model is run for four years and the results of the fourth year simulation of the coupled physical-biological model are analysed in detail.

Spatial and temporal variations of Chlorophyll (Chl), Primary Productivity (PP), Zooplankton (Z), Nitrate (N_n), Ammonium (N_r) and Bacteria (B) are examined in detail for the Arabian Sea (AS) and the Bay of Bengal (BOB), because cruise data on these variables are available. All these variables are important in the study of carbon flux across the air-sea interface. Seasonal variation is studied by considering averages in four quarters, namely, South West Monsoon (June, July & August, SWM), North East Monsoon (December, January & February, NEM), Spring Inter Monsoon (March, April & May, SIM) and Fall Inter Monsoon (September, October & November, FIM) (For detailed discussion, refer Sharada et al[11]).

As the present task of analysis consists of, nine experiments and seasonal variability of several variables, we must, out of necessity, leave out some of the details in the interest of clarity. In Fig. 1, the annual average of PP (on the left) and annual average of Chl (on the right) obtained from four numerical experiments, A, D, G and I (refer to Table 2 for parameters and discussion in Model section) are compared with the SeaWiFS climatology (SeaWiFS Home Page) in the last row. It can be noticed that major features of the spatial variation observed in SeaWiFS data like high PP and Chl in the west AS, low PP and Chl in central AS and most parts of BOB are captured by all the four experiments. But spatial variation obtained from exp I is closest to observations. PP is higher in the south coast of India for all simulations compared to SeaWiFS data. This may due to the increased upwelling in this area in the model compared to observations. PP is more for exp G in west AS and central AS compared to other experiments because grazing by zooplankton is less. Spatial variation of PP for experiments D and I look similar since ammonium regenerated by zooplankton is reduced for both experiments and hence regenerated production is less. PP in west AS is more for exp I compared to exp D since zooplankton is less and grazing by zooplankton

is less. Chl is underestimated for all the simulations in AS and BOB. This might be because of constant C:Chl ratio being used for estimating Chl from phytoplankton biomass. There are dynamic models for C:Chl ratio (Geider[19,20]) based on available light, nutrients and temperature, but they have not been implemented here.

Figures 2 and 3 show the comparison of seasonal averages of depth integrated PP in the euphotic zone, in northern Indian Ocean obtained from the same four numerical experiments as in Fig.1 as well as a comparison with SeaWiFS climatology in NEM and SWM respectively. PP is low in whole of BOB during both monsoon seasons, but all model simulations show low PP in east BOB during NEM and SWM. High values of PP in the northern AS due to the availability of nutrients by convective mixing (Madhupratap et al[21]) and low values of PP in BOB seen in the observations as well as SeaWiFS, during NEM is obtained from the model simulations,. As in Fig.1, PP is higher near the south coast of India for all simulations compared to SeaWiFS data.

SeaWiFS data show high PP in the coastal regions of Somalia and Oman and Central AS during SWM which is supported by the nutrients available in the euphotic zone by coastal upwelling, offshore advection, Ekman pumping and wind-induced mixed-layer deepening (Wiggert et al[22]). All the model experiments show high PP in the west AS but overestimate the PP in the east, west and south coastal regions of India. PP from experiments D and I in central AS is less than the observed values.

Lower values of PP is observed during SIM in AS and BOB except in Northern AS than in the SeaWiFS data (Fig. 3). Results of the simulations (in particular, exp D and I) show similar features. During FIM, high PP are observed in the west AS, and low PP are observed in the central AS and BOB. These features are captured by all the numerical experiments. All the model experiments show high PP in the east, west and south coastal regions of India which is not observed in SeaWiFS data. PP from experiments D and I in central Arabian Sea are less than the observed values.

The spatial variation of surface Chl during four seasons, compared with SeaWiFS climatological data are shown in Figures 4 and 5. All model simulations underestimate Chl during NEM and SWM in AS and BOB. One reason for this is the

absence of a dynamic C:Chl ratio as mentioned earlier. Higher surface Chl values north of 10°N in AS obtained from all experiments are due to high concentrations of nutrients and PP as also observed in SeaWiFS data. Low Chl values in the AS south of 10°N agree well with SeaWiFS observations for experiments D and I, during NEM. Phytoplankton blooms with chlorophyll values greater than 1.0
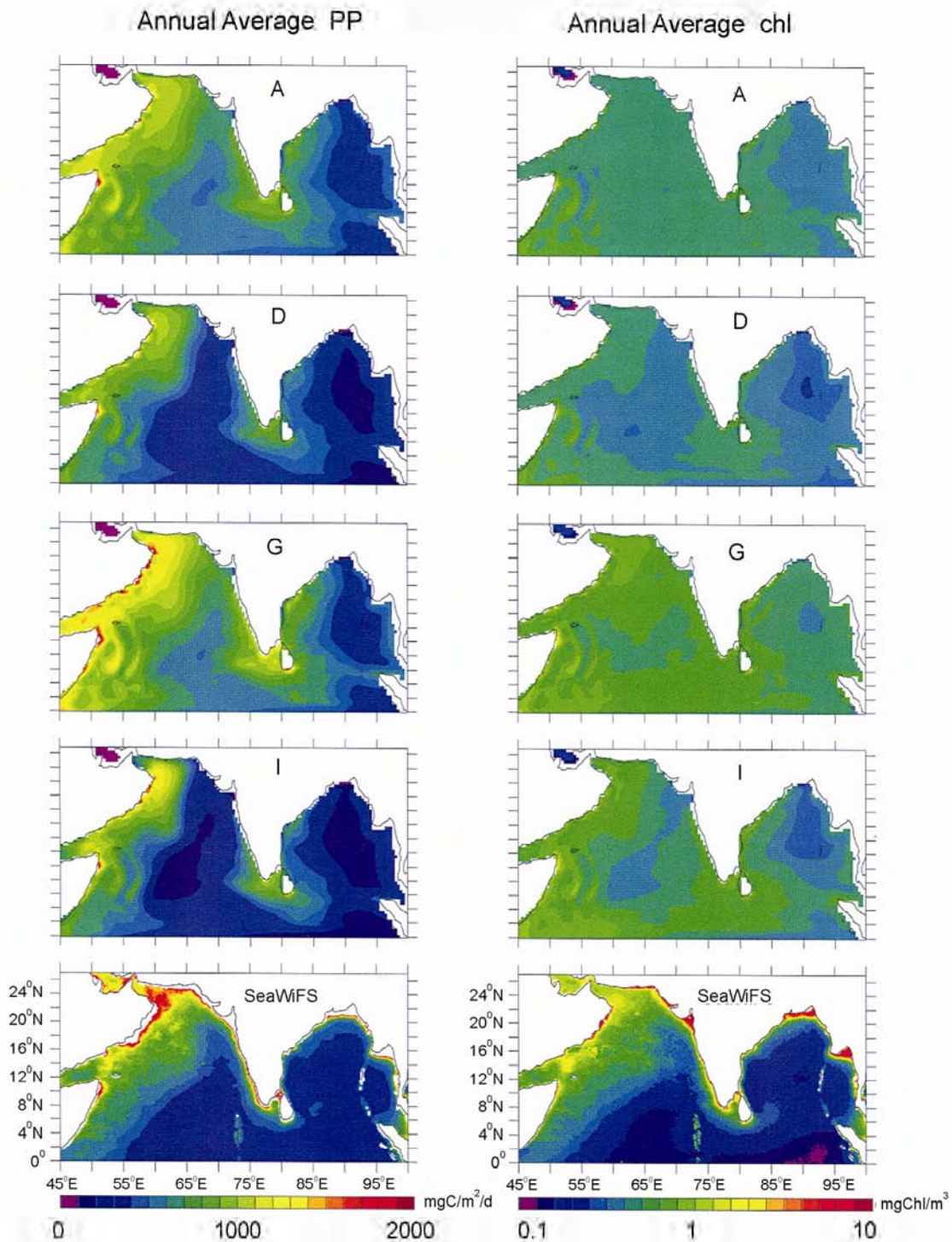
Fig. 1—Annual average PP integrated over 120m (mgC/m²/day) and Annual average of Chl (mgChl/m²) obtained from four numerical experiments (expD, expG, expI and expA) compared with SeaWiFS climatology data.
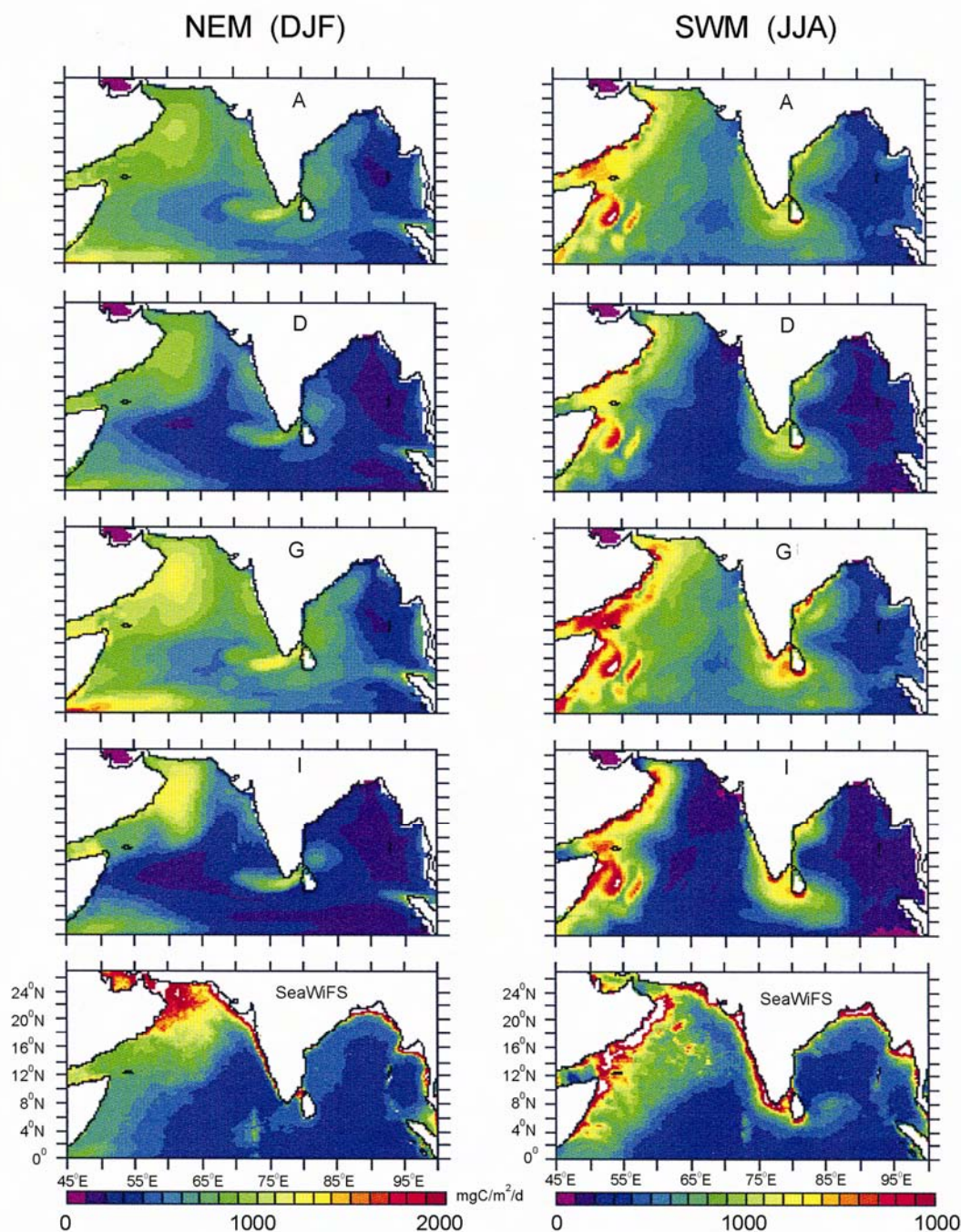
Fig. 2—Seasonal average PP integrated over 120m (mgC/m^2/day) obtained from four numerical experiments (expD, expG, expI and expA) during NEM and SWM compared SeaWiFS climatology data.

mg/m^3 extending from the coast of Somalia and Arabian Peninsula into the central AS, and also along the west coast of India are observed during SWM (Fig. 4, right panels). Higher concentrations of Chl observed between 5°N and 10°N and around 85°E (east of Srilanka) is captured by exp I. Chl values are overestimated by the model in the offshore regions of BOB, north of 10°N. exp I seems to perform best when compared to SeaWiFS.

Lower values of Chl are observed during SIM in the AS and BOB except in northern AS in SeaWiFS data (Fig. 5, left panels). Spatial variation of Chl during SIM obtained from all the model simulations agree fairly well with the SeaWiFS data except in south coastal region of India. Higher
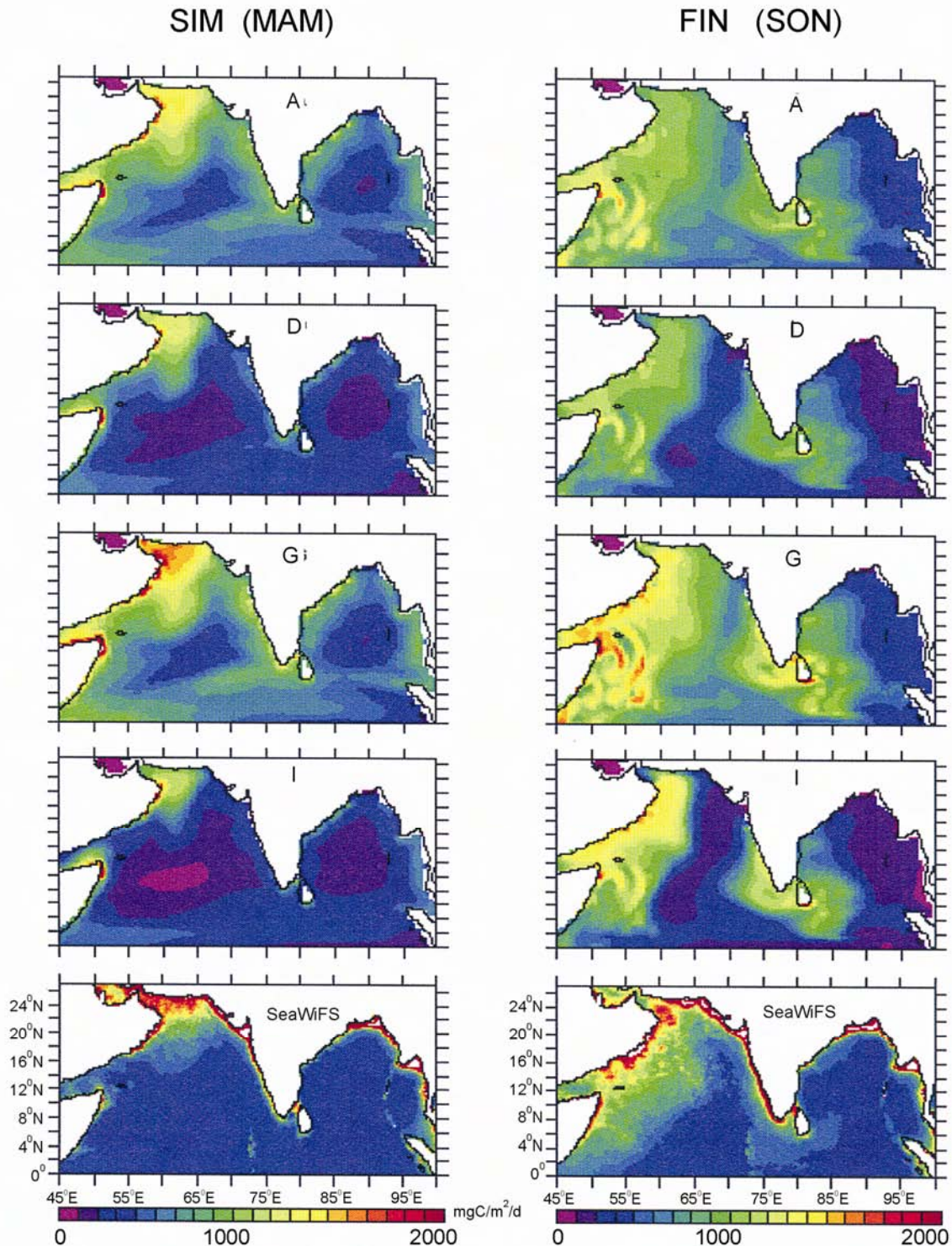
Fig. 3—Seasonal average PP integrated over 120m (mgC/m^2/day) obtained from four numerical experiments (expD, expG, expI and expA) during SIM and FIM compared SeaWiFS climatology data
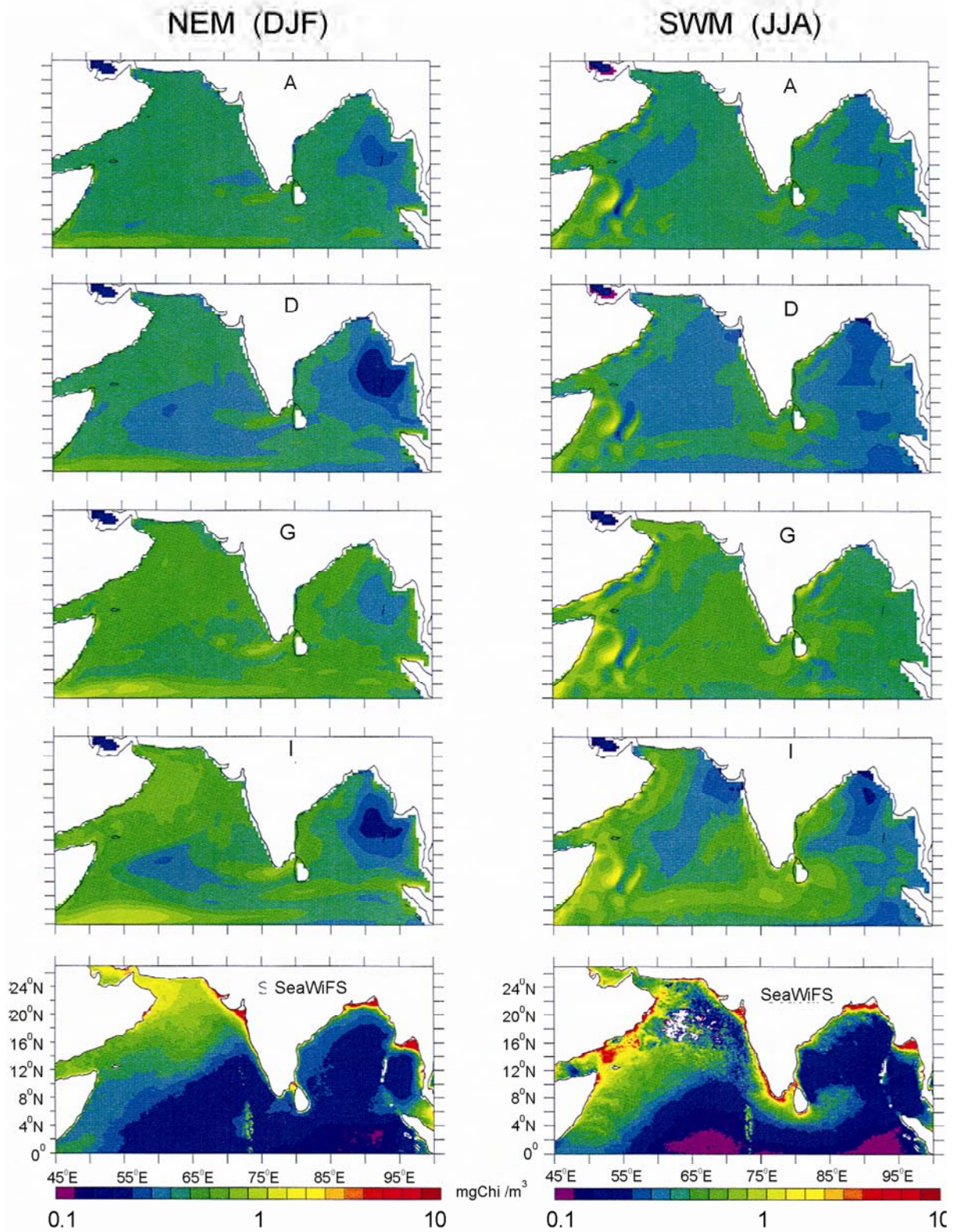
Fig. 4—Seasonal average Chl averaged over 30m (mgChl/m³) obtained from four numerical experiments (expD, expG, expI and expA) during NEM and SWM compared SeaWiFS climatology data
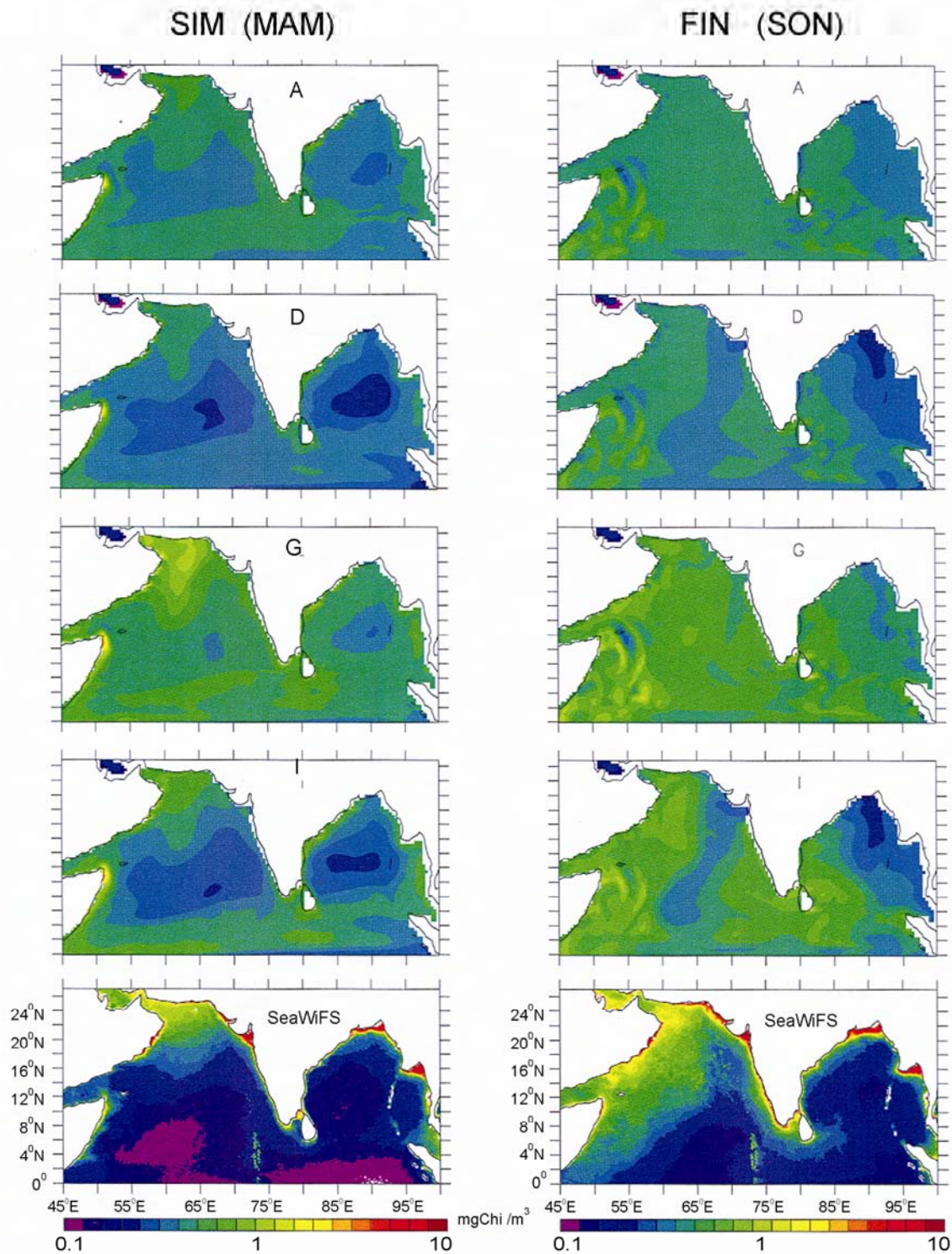
Fig. 5—Seasonal average Chl averaged over 30m (mgChl/m³) obtained from four numerical experiments (expD, expG, expI and expA) during SIM and FIM compared SeaWiFS climatology data

values of Chl are observed during FIM near the coast of India and Oman which is obtained from all numerical simulations. All the simulations overeastimate Chl compared to SeaWiFS data in the east, west and south coastal regions of India.

In general, PP and Chl are less in BOB compared to AS for all the seasons. Lower values of PP and Chl are observed in the central AS and BOB during

all seasons. The basin-wide variation of PP and Chl show that high PP and Chl are seen in North-Western AS and southern coast of India for all the seasons. Although the basin-wide variation of PP from all the experiments agrees well with the PP data obtained from SeaWiFS, exp I is closest to the observations.

Next we focus on specific sites occupied by JGOFS and the WHOI buoy (time series) to study the temporal variability in greater detail. We also show all the nine experiments (A-I) as opposed to only four shown in Figures 1 to 5. Figure 6 shows the seasonal variation of monthly averages of depth integrated PP (left panels) and Chl (right panels) obtained from nine model simulations compared with the snapshots of JGOFS cruise data at S4 (17.2°N, 59.8°E), S7 (16°N, 62°E), S11 (14.5°N, 65°E) and S15 (10°N, 65°E) (Note the sites are increasingly offshore from the Oman coast), and with data obtained from buoy located at a station near S7 in AS. At S4 and S7, exp I is close to US JGOFS cruise data. At S11, experiments A, F and G are close to JGOFS data during all seasons except during August-September. At S15, all model simulations underestimate PP during January, March and August. High PP observed during the JGOFS cruises at S7, S11 and S15 during SWM are not seen in any of the simulations.

At S7, monthly average values of depth integrated PP are also compared with the daily average values of depth integrated PP obtained from buoy data (Marra *et al*[2]). Although this comparison suffers from averaging bias (daily vs monthly mean), we prefer to show it in the interest of capturing the trend. Many of the numerical simulations could capture the bloom observed in buoy data during February-March. The peak values of PP are obtained from some of the simulations during August and October whereas peak values are seen in observations during September and November. Many numerical simulations show low PP during April-May as seen in buoy data. The blooms obtained from numerical simulations are weaker during August-September compared to February, but blooms seen in buoy data during August-September and December are much higher than those obtained during February.

Another feature that can be seen is the decrease in depth integrated PP as we go offshore (from S4 to S15) from the Oman coast. Between the simulation experiments, exp I seems to be the lowest in PP and exp G is the highest. The range between exp I and G can be qualitatively explained by (a) the

reduction of ammonium due to lower regeneration in exp I and (b) reduced grazing by zooplankton in exp G.

Depth integrated Chl is compared with the snapshots of JGOFS cruise data in the right panels of Fig. 6. The experiments are generally spread on either side of the observations. The NEM and SWM blooms as well as low Chl during SIM are captured by all simulations. There is no clear envelope of simulations. Though it is clear that exp C has lowest value, which is linked to lower ammonium fraction of zooplankton excretion (γ_3), experiments B and G, which have lower zooplankton growth seem to form the upper bound.

At S7, many of the numerical simulations capture the bloom observed during February-March. Peak values of Chl are obtained from the simulations during August and October whereas peak values are seen in observations during September and November. The numerical simulations show low values of Chl during April-June as seen in buoy data but all model simulations overestimate Chl during this season. Blooms obtained from numerical simulations are weaker during August compared to February, but blooms seen in buoy data during September and February are of the same magnitude.

The depth profiles of PP and Chl at two stations in AS, S4 (Fig. 7), S7 (Fig. 8) and two in BOB (9°N, 88°E) (Fig. 9) and (15°N, 88°E) (Fig. 10) are shown for several cruises. The behavior at S4 and S7 is consistent with what is seen in the top two panels of Fig. 6, while exp I seems to perform well on most of the cruises, the SIM (April) values are much smaller than observations.

At S4 (Fig. 7), Chl from experiments D and A agree well with the cruise data during August, November and December. Deep chlorophyll maximum observed during April is captured by experiments B, D and I, the highest value of Chl obtained from exp I is close to observations. Deep chlorophyll maximum observed during January and September are not captured by any of the simulations, while deep chlorophyll maximum seen in many simulations during November, is not observed in the cruise data. The behavior of the experiments at S4 is consistent with what was seen in the spatial results of Figures 1 to 5. The reduction of zooplankton concentration by the reduction of the grazing rates (in experiments B and G), or the increase in zooplankton mortality (exp E) or increasing export (exp D) have led to high Chl, while experiments C and H have resulted in lower ammonium (regenerated by zooplankton) and hence lower Chl.
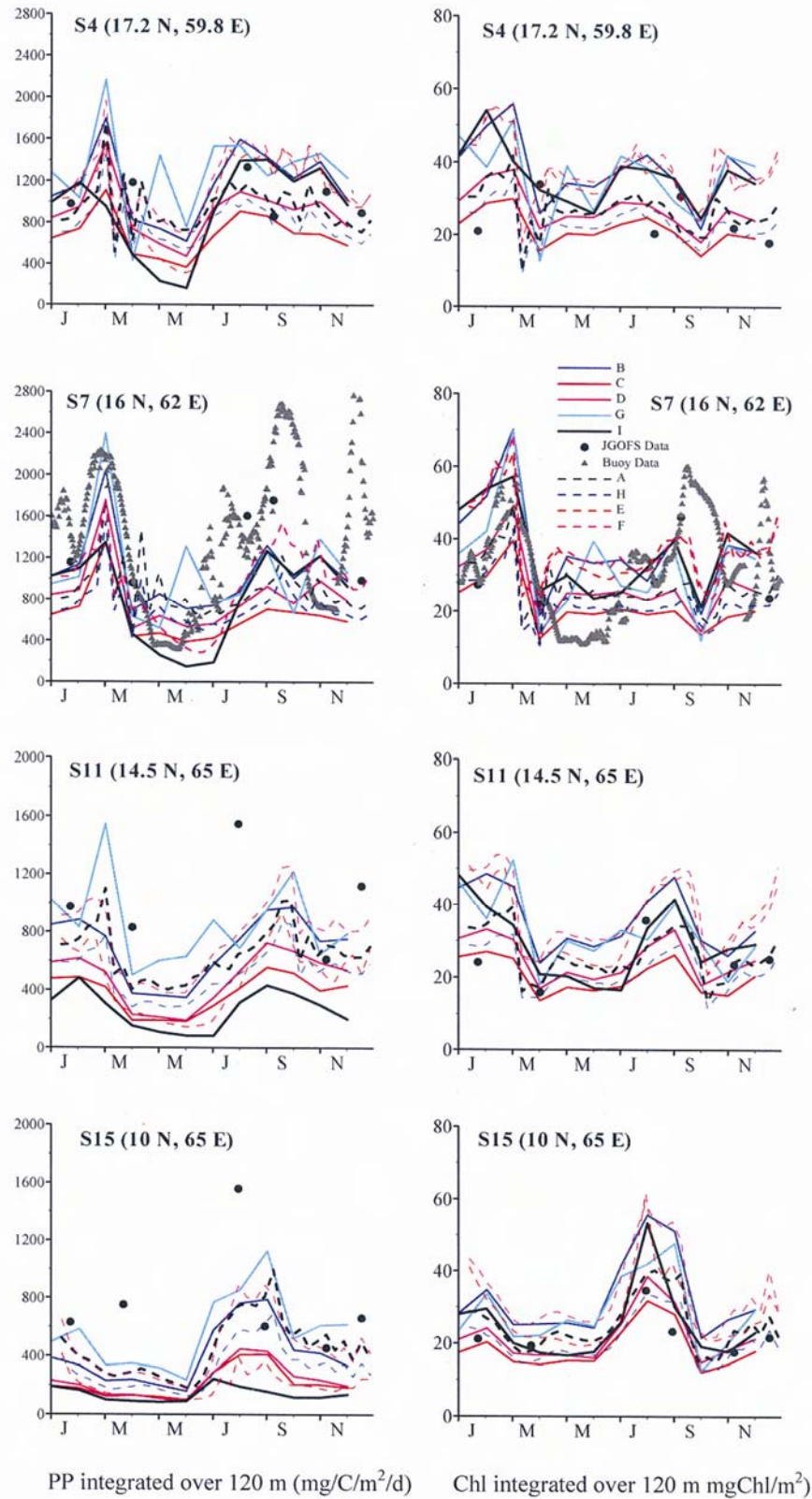
Fig. 6—Seasonal variation of PP integrated over 120m (mg C/m^2/day) and Chl integrated over 120m (mgChl/m^2) obtained from nine numerical simulations compared with US JGOFS cruise data at four stations S4, S7, S11 and S15 and buoy data at S7 in AS.
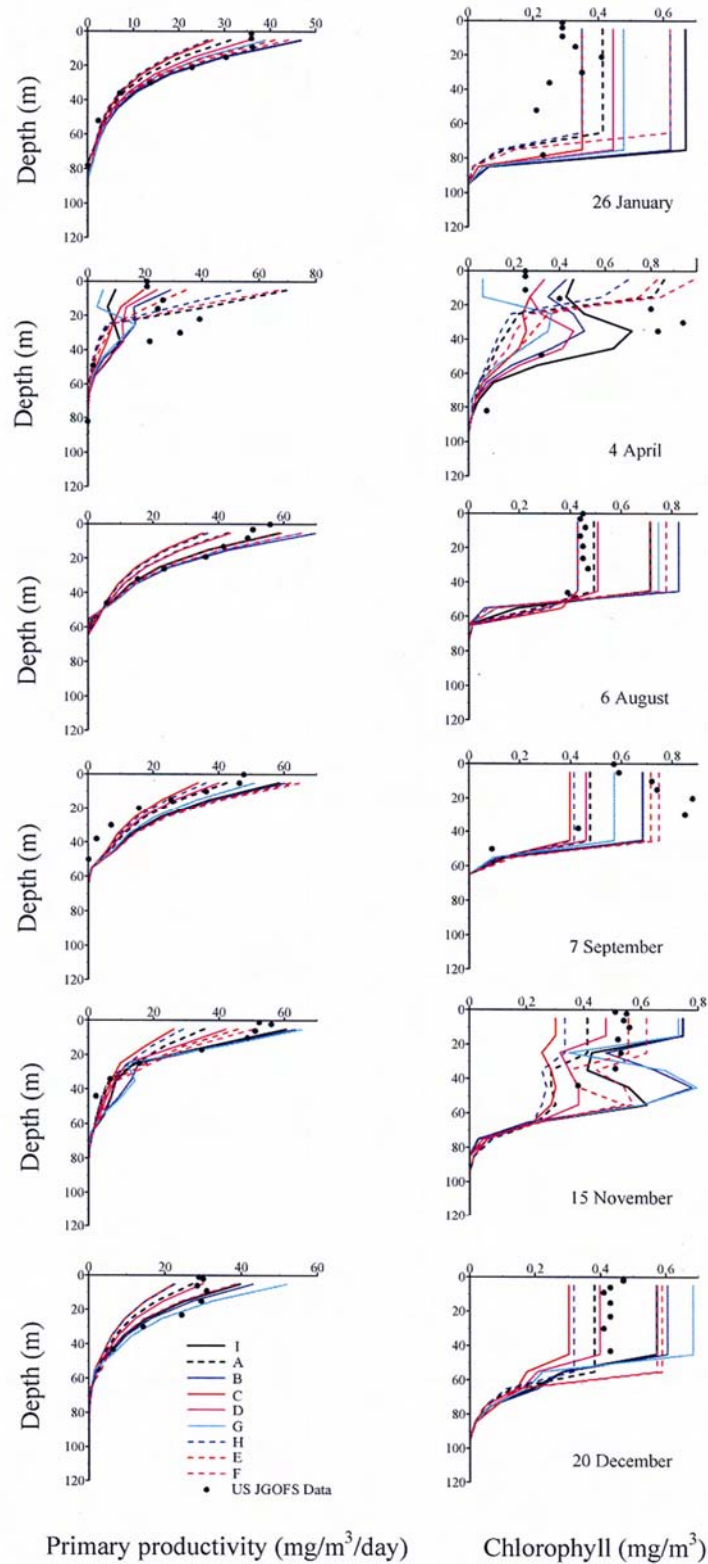
Fig. 7—Profiles of PP (mg C/m^3/day) and Chl (mgChl/m^3) obtained from nine numerical simulations compared with US JGOFS cruise data during six times over a year at S4 in AS.
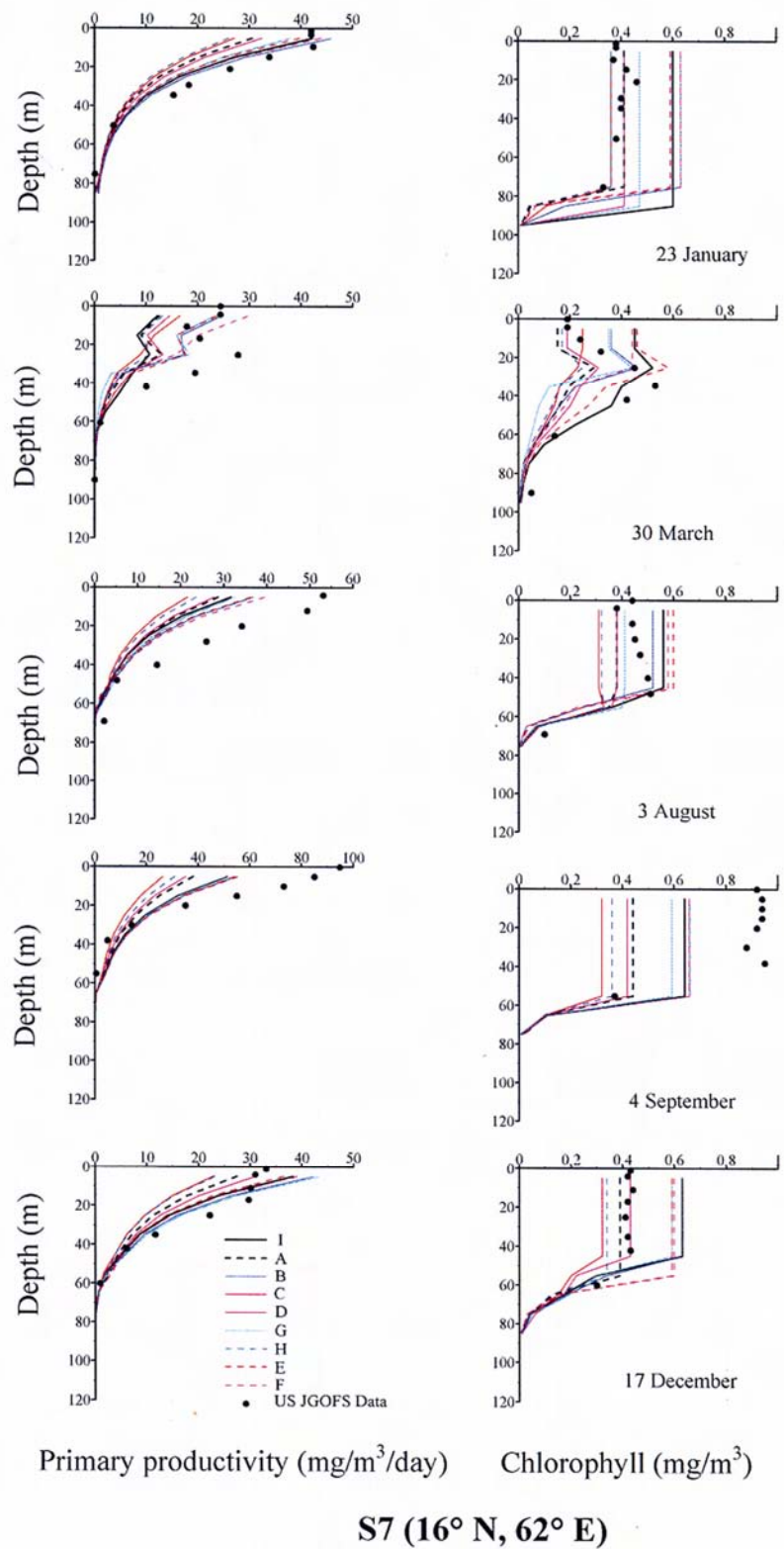
Fig. 8—Profiles of PP (mg C/m³/day) and Chl (mgChl/m³) obtained from nine numerical simulations compared with US JGOFS cruise data during six times over a year at S7 in AS.
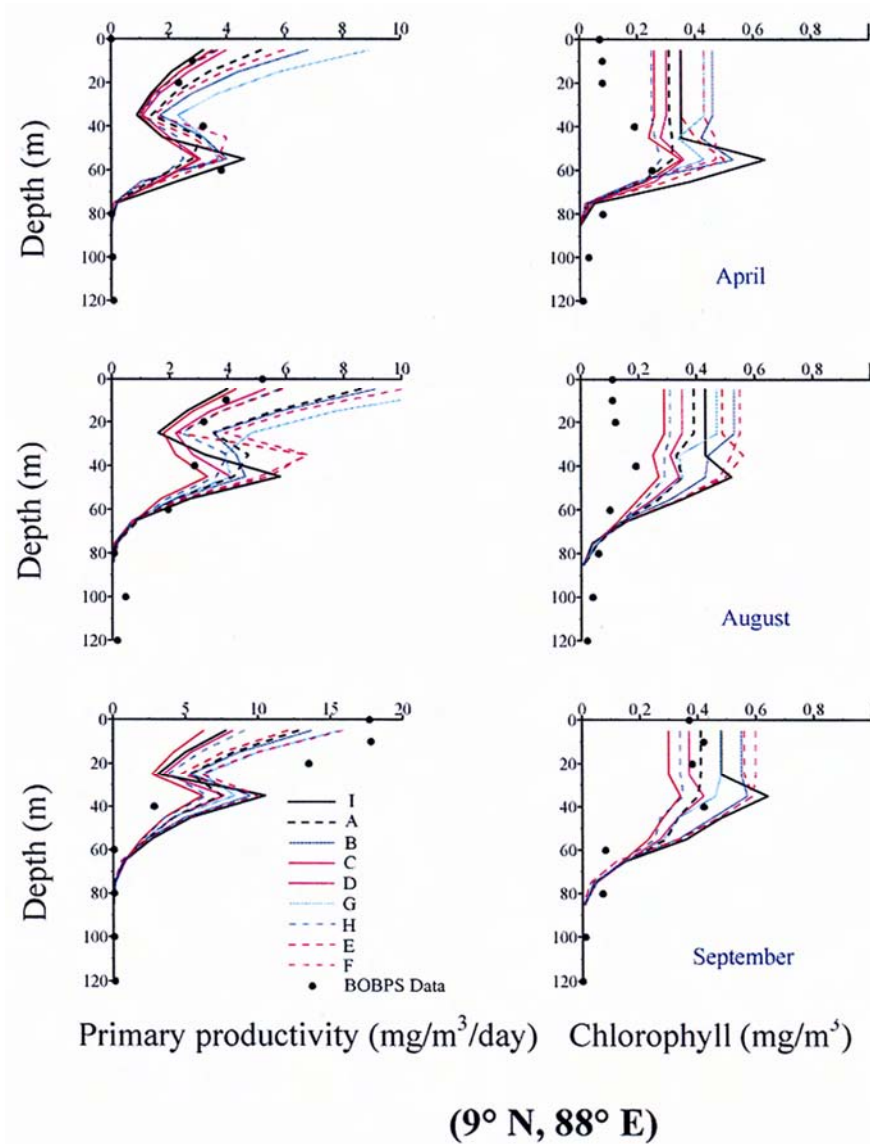
Fig. 9—Profiles of PP (mg C/m^3/day) and Chl (mgChl/m^3) obtained from nine numerical simulations compared with BOBPS cruise data during three times over a year at (9°N, 88°E) in BOB.

At S7 (Fig. 8), PP obtained from a few of the simulations (in particular, exp I) agrees well with the observations during January and December, but none of the simulations could capture the high PP during August-September. The subsurface maximum of PP during March is captured by exp I and its magnitude is less than the observed values. Chl values obtained from experiments D and A agree well with the cruise data during January, August and December. Deep chlorophyll maximum observed during March is captured by experiments B, G, E, F and I (When zooplankton concentration is reduced either by decreasing the asymptotic grazing rate or by increasing the half-saturation constant for grazing or by increasing the grazing by higher predators on zooplankton) and high values of Chl obtained from cruise data during September is not captured by any of the numerical experiments. The reason for low Chl in September may be due to high zooplankton concentration leading to increased grazing of phytoplankton. Again, the simulation experiments are consistent with what was seen in Fig. 7 for S4.

At (9°N, 88°E) BOB station (Fig. 9), we have oligotrophic conditions and PP from some of the simulations match well with BOBPS cruise data during April and August, but not during September.
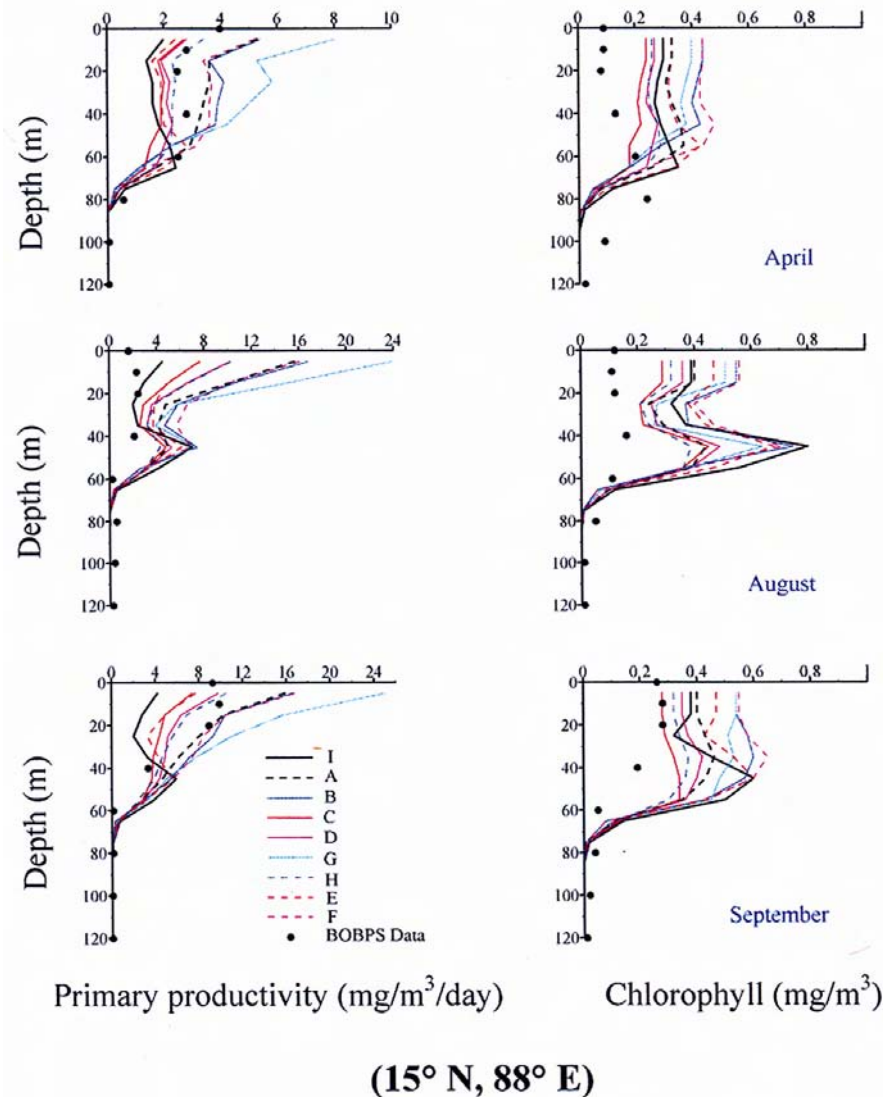
Fig. 10—Profiles of PP (mg C/m³/day) and Chl (mgChl/m³) obtained from nine numerical simulations compared with BOBPS cruise data during three times over a year at (15°N, 88°E) in BOB.

The subsurface maximum PP shown by all simulations during August and September is not observed during BOBPS cruises. High PP observed in BOBPS at the surface during September are closest to the values obtained by experiments F and G. Lower PP obtained by experiments C, H, D and I are close to observed values during April and August. Chl obtained from experiments D and A agree well with the cruise data during September. All model experiments overestimate Chl during April and August. At (15°N, 88°E) (Fig.10), PP obtained from some of the simulations match well with BOBPS cruise data during all seasons. PP obtained by experiments A, C, D, H and I are close to observed values during April. Chl obtained

from exp C are closest to the observations during April and September.

Figures 9 and 10 show that Chl obtained from all the simulations is higher than observations during April (SIM) and August (SWM), though the depth of deep chlorophyll maximum obtained from simulations agrees with the observations.

The profiles of nitrate (N_n) from all the experiments are compared with JGOFS data during six times over a year at stations S4 and S7 in Fig. 11. Nitrate concentrations in the upper ocean obtained from many of the simulations agree well with the observed data during all seasons and at both stations. Below 100m, nitrate concentrations obtained from experiments A, C and H are close to
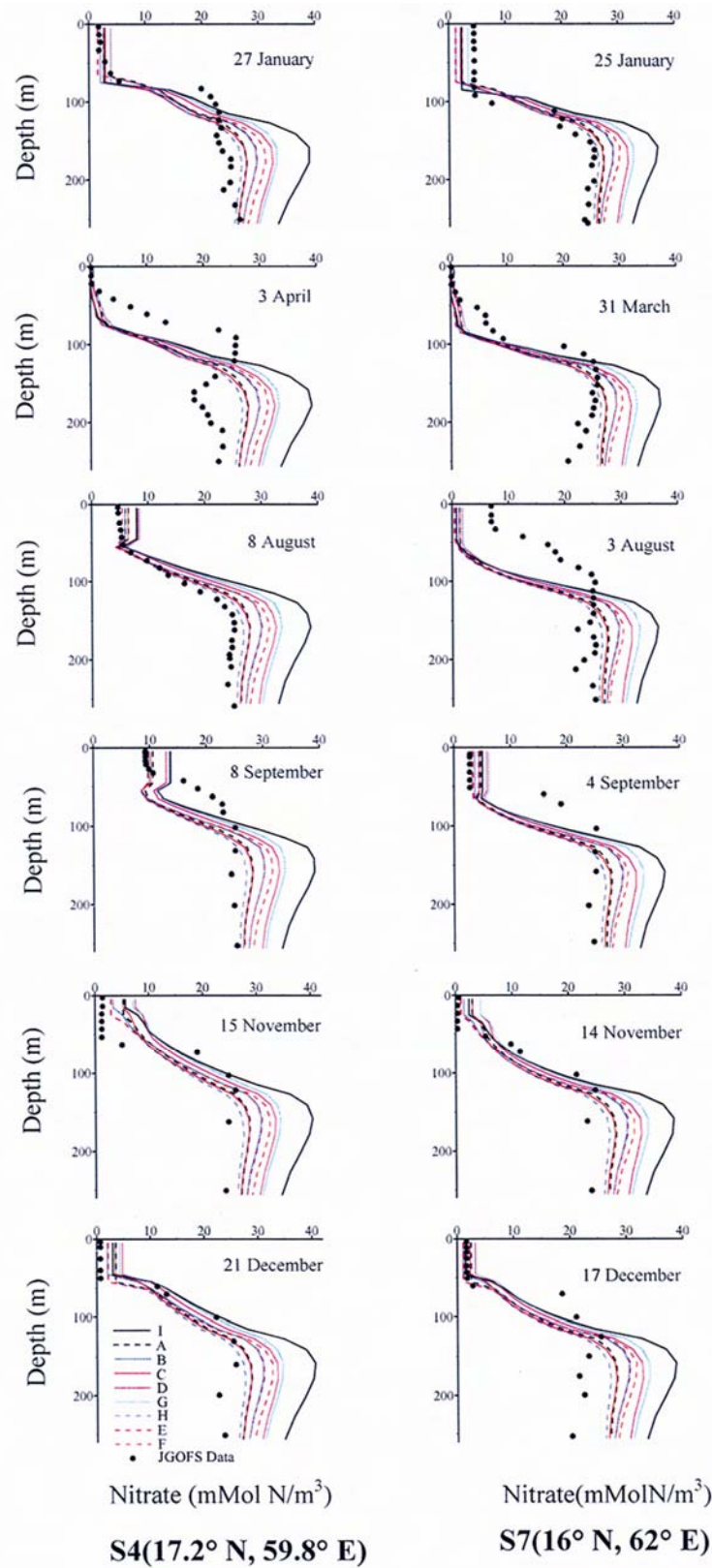
Fig. 11—Profiles of Nitrate (m Mol N/m³) obtained from nine numerical simulations compared with US JGOFS cruise data during six times over a year at S4 and S7 in AS.

observations. Nitrate concentration obtained from exp I are very high below 100m. Nitrate concentration below 100m is influenced by the remineralization and nitrification processes. More studies are required to be done on modeling of remineralization processes below the euphotic zone. Earlier studies (Anderson *et al*[23]) have also encountered this difficulty and resorted to restoring nitrate to observations below

100m. At S4, observations show a minimum value of nitrate below 100m during April, which is not captured by any of the simulations. Depth of nitracline obtained from simulations is more than the observations during April and September. At S7, depth of nitracline obtained from simulations is more than the observations during August and September and is less than the observed data during January.
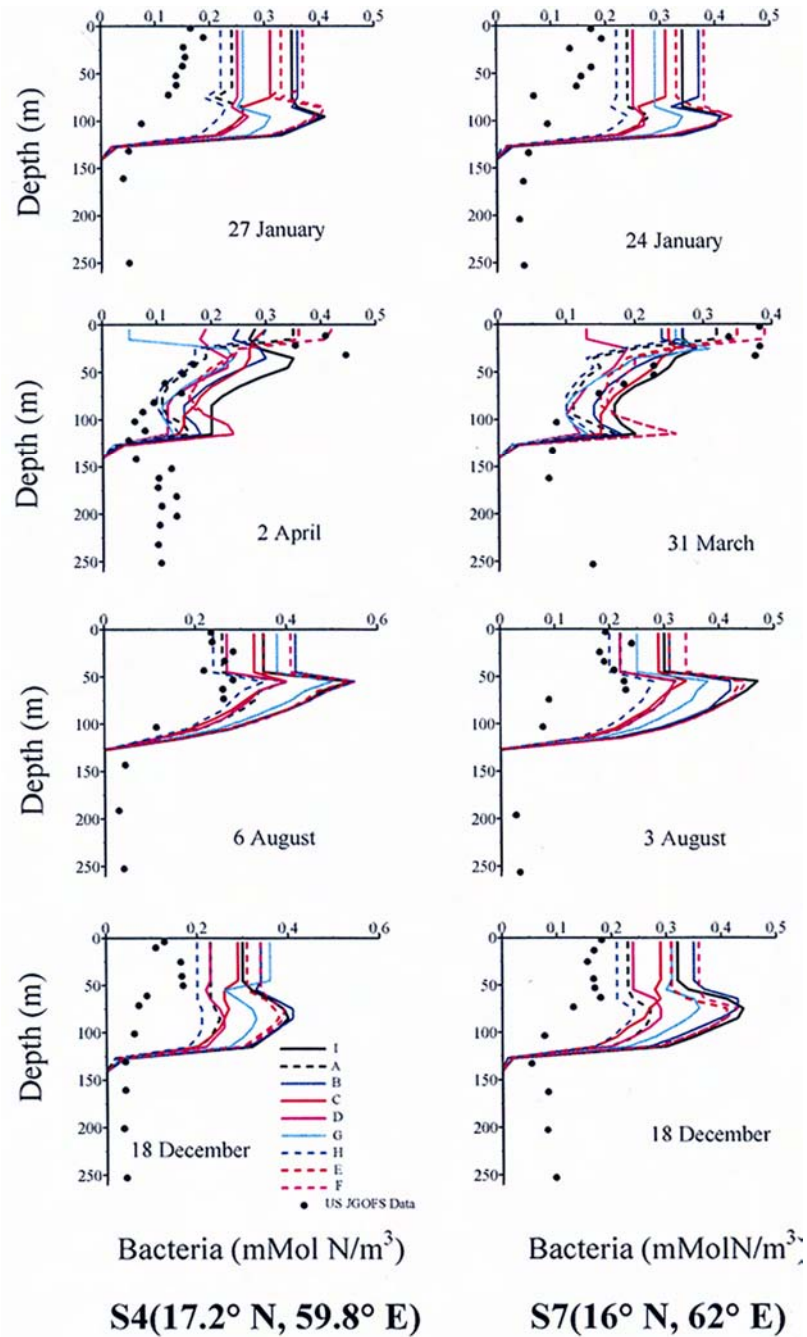
Fig. 12—Profiles of B (m Mol N/m^3) obtained from nine numerical simulations compared with US JGOFS cruise data during four times over a year at S4 and S7 in AS

Figure 12 shows the profiles of bacteria obtained from simulations compared with the JGOFS cruise data during four seasons at S4 and S7. Almost all the experiments overestimate the bacterial biomass in the euphotic zone during all seasons except during March-April because of high concentrations of ammonium in the euphotic zone. Exp I agrees well with the JGOFS cruise data during March-April at depths < 140m. The bacterial biomass obtained from simulations is zero below 140m (because of the model formulation below the euphotic zone), though bacterial biomass is nonzero below 140m in the observations. The subsurface maximum of bacteria obtained from many of the simulations during all seasons is observed only during a few of the JGOFS cruises. Lower values of bacterial biomass obtained for experiments A, D and H (regeneration of ammonium by zooplankton is less and hence growth of bacteria due to ammonium is less) during January and August are close to observed values at a few stations in Arabian Sea. Higher values of bacteria are obtained from experiments B, F, G and I during all seasons since grazing by zooplankton on bacteria is less (zooplankton is less). These values are close to observations during April when bacterial biomass is high compared to other seasons.

Concentration of bacteria and bacterial production are high compared to observations since zooplankton and ammonium concentrations are high compared to JGOFS cruise data at all stations during all seasons. When zooplankton concentration is high, mortality of zooplankton, ammonium and dissolved organic nitrogen fractions of zooplankron excretion are also high. These lead to higher ammonium and dissolved organic nitrogen, which are taken up by bacteria.

Table 3 shows the depth integrated (upto 200m) concentration of zooplankton. Exp I results during SWM at S2 (18°N, 58°E), S4, S7, S11 and S15 are higher than those during NEM (as in Smith *et al*[24]). Also, the amount of zooplankton decreases with distance from the shore and S15 has the lowest values of zooplankton during all seasons in the simulations. Therefore the observational trend in depth integrated values of zooplankton with respect to the distance from the shore is captured well in simulation results obtained from exp I. However, the magnitude of values obtained from simulations (includes all size classes) can not be compared with cruise data because observations include only zooplankton > 200 microns.

Conclusions

An earlier study (Sharada *et al*[10]) showed that the choice of the kinetic relation and the values of model parameters have a significant effect on the dynamics of the ecosystem. These studies have been extended to include a detailed parameter sensitivity study by varying the parameters influencing the zooplankton growth and regeneration of ammonium by zooplankton and bacteria.

Detailed analysis of concentrations of tracers and primary productivity is done for nine numerical experiments. On a basin-wide scale, high primary productivity and chlorophyll in North-Western Arabian Sea and southern coast of India in all the seasons are seen in models. Of all the experiments, exp I (Table 2) seems to be the best in capturing low primary productivity and chlorophyll during SIM, regions of high primary productivity and chlorophyll during SWM, NEM and FIM in Arabian Sea and Bay of Bengal.

Table 3—Zooplankton integrated over 200m (mMolC/m^2)

ttn043	January								
Station	expA	expB	expC	expD	expE	expF	expG	expH	expI
S2	91.41	122.17	114.87	94.29	80.21	122.77	86.38	92.33	82.75
S4	89.56	120.22	111.22	91.74	77.62	119.38	92.93	90.1	78.3
S7	88.66	120.59	110.36	91.31	77.43	116.22	114.43	88.59	76.19
S11	75.71	97.34	79.98	66.18	55.43	95.33	93.01	72.62	49.87
S15	44.35	45.55	30.07	22.53	18.27	47.83	62.67	35.27	11.53
Ttn049	July-August								
Station	expA	expB	expC	expD	expE	expF	expG	expH	expI
S2	137.39	199.3	161.42	137.87	134.44	192.05	179.29	135.6	136.79
S4	1.5.85	145.03	119.92	104.27	103.99	144.06	138.8	1.366	101.89
S7	89.77	116.73	106.13	87.27	68.78	115.6	114.13	88.75	63.39
S11	69.81	87.2	75.51	57.4	25.86	87.67	88.63	68.12	5.35
S15	72.39	85.59	62.19	45.21	17.08	83.59	94.89	64.11	2.16

Seasonal variation of depth integrated values of PP and Chl at S7 in AS show that almost all the numerical experiments capture the trend in observations (Buoy Data) during the January-February and March-May but none of the simulations could capture high PP during July-September and December as seen in buoy data at S7.

Depth profiles of PP from many of the present simulations agree well with the JGOFS cruise data at several stations in AS and BOBPS cruise data in BOB, during all seasons except during July-September for some stations. Smaller values of primary productivity are obtained when some of the parameters are changed to reduce the regeneration of ammonium by zooplankton. PP from exp I are closest observations at many stations in AS and BOB.

Depth profiles of nitrate obtained from almost all the simulations agree well with the observed data (US JGOFS cruise data) in upper ocean (upto 100m). Below the nitracline, many of the simulations overestimate the nitrate concentration. Nitrate obtained from the numerical simulations where regeneration of ammonium by zooplankton is reduced, are closer to observations. Depth profiles of bacteria obtained from nine numerical experiments during four seasons at two stations in Arabian Sea overestimate the bacterial concentration during all seasons except during March-April when compared with the JGOFS cruise data. The values of bacteria obtained from exp H are closest to observations during all seasons.

Present study infers the importance of (a) control by zooplankton grazing and (b) regeneration of ammonium in controlling the ecosystem dynamics of AS and BOB. We have isolated the set of ecosystem parameters which has great potential for application for further studying the marine productivity and carbon dioxide transfer in the Indian Ocean.

Acknowledgements

References

1   Barber, R.T., Marra, J., Bidigare, R.C., Codispoti, L.A., Halpern, D., Johnson, Z., Latasa, M., Goericke, R., and Smith,S.L.,,. Primary productivity and its regulation in the Arabian Sea during 1995, *Deep Sea Research II,* 48 (2001) 1127–1172.

2   Marra, J., T. D. Dickey, C. Ho, C. S. Kinkade, D. E. Sigurdson, R. A. Weller, and R. T. Barber, Variability in primary production as observed from moored sensors in the central Arabian Sea in 1995, *Deep Sea Research II*, 45 (1998) 2253-2267.

3   Prasanna Kumar, S., P. M. Muraleedharan, T. G. Prasad, M. Gauns, N. Ramiah, S. N. de Souza, S. Sardesai and M. Madhupratap, Why is the Bay of Bengal less productive during summer monsoon compared to the Arabian Sea?, *Geophysical Research Letters* 29 (24) (2002) 2235

4   Prasanna Kumar, S., M. Nuncio, N. Ramaiah, S. Sardesai, Jayu Narvekar, Veronica Fernandes, and Jane T. Paul, Eddy-mediated biological productivity in the Bay of Bengal during fall and spring intermonsoons, *Deep Sea Research I*, 54 (2007) 1619–1640.

5   Fasham, M. J. R., Ducklow, H. W. and McKelvie, S. M., A Nitrogen-based Model of Plankton Dynamics in the Oceanic Mixed Layer, *Journal Marine Research*, 48 (1990) 591-639.

6   Doney, S.C., Glover, D.M. and Najjar, R.G., A new coupled, one-dimensional biological-physical model for the upper ocean: applications to the JGOFS Bermuda Atlantic time-series study (BATS) site, *Deep-Sea Research II,* 43 (1996) 591–624.

7   Moore, J. K., S. C. Doney, J. A. Kleypas, D. M. Glover and I. Y. Fung, An intermediate complexity marine ecosystem model for the global domain, *Deep-Sea Research II*, 49 (2002) 403–462.

8   Moore, J. K., S. C. Doney, D. M. Glover and I. Y. Fung, Iron cycling and nutrient-limitation patterns in surface waters of the World Ocean, *Deep-Sea Research II*, 49 (2002) 463–507.

9   Swathi, P. S., Sharada, M. K. and Yajnik, K. S., A coupled Physical-biological-chemical model for the Indian Ocean, *Proceedings of Indian Academy of Sciences (Earth and Planetary Sciences)*, 109 (4) (2000) 503-537.

10 Sharada, M. K., Yajnik, K. S. and Swathi, P. S., Evaluation of six relations of the kinetics of uptake by phytoplankton in multi-nutrient environment using JGOFS experimental results, *Deep Sea Research II*, Vol. 14-15 (2005) 1845-2078.

11 Sharada, M. K., Swathi, P. S., Yajnik, K. S. and C. Kalyani Devasena, Role of biology in the air–sea carbon flux in the Bay of Bengal and Arabian Sea, *Journal of Earth System Science*, 117 (4) (2008) 429–447.

12 Pacanowski R C 1995 MOM2 Documentation, User's Guide and Reference Manual. Ver 1.0, *GFDL Ocean Tech. Report No. 3.*

13 Pacanowski, R. C. and G. Philander, Parametrization of vertical mixing in numerical models of the tropical ocean, *Journal of Physical Oceanography*, 11 (1981) 1442-1451.

14 Levitus, S., T. P. Boyer and J. Antonov, *World Ocean Atlas*; Vol. 4 (1994), NESDIS, Washigton.

15 Sarmiento, J. L., Slater, R. D., Fasham, M. J. R., Ducklow, H. W., Togglweiler, J. R. and Evans, G. T., A seasonal three-dimensional ecosystem model of nitrogen cycling in the

north Atlantic euphotic zone, *Global Biogeochemical Cycles,* 7(2) (1993) 417-450.

16 Wroblewski, J. S., A model of phytoplankton plume formation during variable Oregon upwelling, *Journal of Marine Research*, 35 (1977) 357-394.

17 Yajnik, K. S. and M. K. Sharada, Ammonium Inhibition of Nitrate Uptake by Phytoplankton: A New relation Based on Similarity and Hyperbolicity, *Current Science,* 85 (8) (2003) 1180-1189.

18 McCarthy, J. J., C. Garside and J. L. Nevins, Nitrogen dynamics during the Arabian Sea northeast monsoon, *Deep-Sea Research II*, 46 (8-9) (1999) 1623-1664.

19 Geider, R.J., MacIntyre, H.L. and Kana, T.M., A dynamic regulatory model of phytoplanktonic acclimation to light, nutrients, and temperature, *Limnology and Oceanography,* 43 (4) (1998) 679-694.

20 Geider, R.J., MacIntyre, H.L. and Kana, T.M., Dynamic model of phytoplankton growth and acclimation: Responses of the balanced growth rate and the chlorophyll a:carbon ratio to light, nutrient-limitation and temperature, *Marine Ecology Progress Series*, 148 (1-3) (1997) 187-200.

21 Madhupratap, M., Prasanna Kumar, S., Bhattathiri, P.M.A., Kumar, M.D, Raghukumar, S., Nair, K.K.C. and Ramaiah, N., Mechanism of the biological response to winter cooling in the northeastern Arabian Sea, *Nature,* 384 (1996) 549-552.

22 Wiggert, J. D., Murtugudde, R. G. and Christian, J. R., Annual ecosystem variability in the tropical Indian Ocean: Results of a coupled bio-physical ocean general circulation model, *Deep Sea Research II*, 53 (2006) 644-676.

23 Anderson, T.R., Ryabchenko, V.A., Fasham, M.J.R., and Gorchakov, V.A., Denitrification in the Arabian Sea: A 3D ecosystem modeling study, *Deep Sea Research Part I,* 54 (2007) 2082-2119.

24 Smith, S., Roman, M., Prusova, I., Wishner, K., Gowing, M., Codispoti, L. A., Barber, R., Marra, J. and Flagg, C., Seasonal response of zooplankton to monsoonal reversals in the Arabian Sea, *Deep Sea Res. II*, 45 (1998) 2369-2403.

Appendix I

Equations of the Biological Model

The biological model has seven ecosystem conservation equations of Phytoplankton P, Zooplankton Z, Bacteria B, Nitrate N_n, Ammonium N_r, Dissolved Organic Nitrogen N_d and detritus N_p. These conservation equations have advective and diffusive terms of the same form as in the temperature and salinity. Their source-minus-sink terms (SMS) are given below.

$$SMS(P) = (1 - \gamma_1)\,\overline{J}(z,t)\left[Q_1(N_n, N_r) + Q_2(N_r)\right]P - \mu_1 P - G_1 \tag{A1}$$

$$SMS(Z) = \gamma_2\left(G_1 + G_2 + G_3\right) - (\mu_2 + \mu_5)Z \tag{A2}$$

$$SMS(B) = U_1 + U_2 - G_2 - \mu_3 B \tag{A3}$$

$$SMS(N_n) = -\overline{J}(z,t)\,Q_1(N_n, N_r)\,P \tag{A4}$$

$$SMS(N_r) = \left[\gamma_3\mu_2 + (1-\gamma_4)\mu_5\right]Z + \mu_3 B - J(z,t)\,Q_2(N_r)\,P - U_2 \tag{A5}$$

$$SMS(N_d) = \gamma_1\overline{J}(z,t)\left(Q_1(N_n, N_r) + Q_2(N_r)\right)P + (1-\gamma_3)\mu_2 Z + \mu_4 N_p - U_1 \tag{A6}$$

$$SMS(N_p) = \mu_1 P + (1-\gamma_2)\left(G_1 + G_2 + G_3\right) - G_3 - \mu_4 N_p - \omega_s \partial N_p / \partial z \tag{A7}$$

where

P	Phytoplankton
Z	Zooplankton
B	Bacteria
N_n	Nitrate
N_r	Ammonium
N_d	Dissolved Organic Nitrogen
D	Detritus

Light Limitation Model of Phytoplankton Growth (Fasham *et al* 1990)

$$I(z,t) = I(0,t)\exp\left(k_w z - \int_z^0 k_c P dz\right) PAR \tag{A8}$$

$$V_p = ab^{cT} \tag{A9}$$

$$J(z,t) = \frac{V_p \alpha I(z,t)}{\left[V_p^2 + (\alpha I(z,t))^2\right]^{0.5}} \tag{A10}$$

$$\bar{J}(z,t) = \frac{1}{z_k - z_{k+1}} \int_{z_{k+1}}^{z_k} J(z,t) dz \tag{A11}$$

Nitrogen Uptake Kinetics

Nitrogen uptake kinetics is modelled by YS Parameterization scheme, which is explained in Section 2.2 (Sharada *et al* 2005).

$$Q_1(N_n, N_r) = \frac{N_n}{k_1 + N_n} \frac{1 + a_1 N_r}{1 + b_1 N_r} \tag{A12}$$

$$Q_2(N_r) = \frac{N_r}{k_2 + N_r} \tag{A13}$$

Grazing Functions (Fasham *et al* 1990)

$$F = p_1 P + p_2 B + p_3 D \tag{A14}$$

$$G_1 = \frac{g p_1 P^2 Z}{k_3 F + p_1 P^2 + p_2 B^2 + p_3 N_p^2} \tag{A15}$$

$$G_2 = \frac{g p_2 B^2 Z}{k_3 F + p_1 P^2 + p_2 B^2 + p_3 N_p^2} \tag{A16}$$

$$G_3 = \frac{g p_3 N_p^2 Z}{k_3 F + p_1 P^2 + p_2 B^2 + p_3 N_p^2} \tag{A17}$$

Bacterial Growth (Fasham *et al* 1990)

$$S = \min(N_r, \eta N_d) \tag{A18}$$

$$U_1 = \frac{V_b N_d}{k_4 + S + N_d} \tag{A19}$$

$$U_2 = \frac{V_b S}{k_4 + S + N_d} \tag{A20}$$